https://dx.doi.org/10.1016/j.enggeo.2019.105240

An elasto-plastic model of unsaturated soil with an explicit degree of saturation dependent CSL

Jian LI, Zhen-Yu YIN, Yu-Jun CUI, Kai LIU, Jian-Hua YIN

J. Li. PhD, School of Civil Engineering, Beijing Jiaotong University, Beijing 100044, P.R. China. (email: jianli@bjtu.edu.cn)

Z.-Y. Yin. Associate Professor, Department of Civil and Environmental Engineering, The Hong Kong Polytechnic University, Hung Hom, Kowloon, Hong Kong. (email: zhenyu.yin@polyu.edu.hk; zhenyu.yin@gmail.com)

Y.-J. Cui. Professor, Ecole des Ponts ParisTech, Laboratoire Navier/CERMES, 6 et 8 avenue Blaise Pascal, 77455 Marne La Vallée, France. (email: yujun.cui@enpc.fr)

K. Liu. PhD Candidate, Department of Civil and Environmental Engineering, The Hong Kong Polytechnic University, Hung Hom, Kowloon, Hong Kong. (email: kevin-kai.liu@connect.polyu.hk)

J.-H. Yin. Chair Professor, Department of Civil and Environmental Engineering, The Hong Kong Polytechnic University, Hung Hom, Kowloon, Hong Kong. (email: jian-hua.yin@polyu.edu.hk)

Corresponding author: Dr. Zhen-Yu Yin, Tel: +852 3400 8470; Fax: +852 2334 6389; Email: zhenyu.yin@polyu.edu.hk; zhenyu.yin@gmail.com

Abstract:

Simulation analysis with a sophisticated model on both contractive and dilative behaviours for unsaturated soils during shear stage is still a challenge. In this paper, an elasto-plastic model with two plastic deformation mechanisms, i.e. compression and shear sliding, for unsaturated soils has been formulated, using the average soil skeleton stress σ'_{ij} as a stress variable and using the void ratio e and the effective degree of saturation S_{re} as state variables. In order to well describe the dilative behaviour for unsaturated soils, different from previous studies, an S_{re}-dependence of critical state line in the e-logp' plane is explicitly implemented by a formula which takes into account the influences of the pore pressures and an additional "bonding" relating to water menisci under unsaturated state. The performances of the new model in reproducing the shear strength and the dilative and contractive behaviour of unsaturated soil are evidenced by simulating triaxial tests on silty sand, Speswhite kaolin and Jossigny silty clay.

Keywords: compression; shear sliding; degree of saturation; critical state; unsaturated soils

Introduction

Many natural and engineering disasters under unsaturated zone, i.e., slope failure, loss of bearing capacity for foundation ground, are closely relating to the weakening of shear strength for soil from unsaturated to saturated states due to many environmental factors (e.g., Huat et al., 2006; Tsai et al. 2008; Tang et al. 2015; Vo and Russell 2016). For instance, the water content and suction change of soil due to rainfalls will influence significantly the peak strength and residual strength of unsaturated soil (Bishop, 1959; Cui and Delage 1996; Cui et al. 2015; Lyu et al. 2018).

The peak strength is related to the ultimate critical state and the dilative behaviour of soil (Schofield 2006; 2008). The experimental investigations of dilative behaviour for various types of unsaturated geo-materials have been carried out extensively by direct shear tests and triaxial shear tests in nearly two decades (e.g. Cui and Delage 1996; Chiu and Ng 2003; Matsuoka et al. 2002; Cattoni et al. 2005; Futai and Almeida 2005; Pineda and Colmenares 2006; Zhan and Ng 2006; Thu et al. 2007; Estabragh and Javadi 2008, 2014; Ajdari et al. 2010; Fern et al. 2016; Kim et al. 2016; Ma et al. 2016; Ng et al. 2016). These experimental investigations illustrated that the shear-dilative behaviour for unsaturated geo-materials is an important feature and dependent on not only the stress level and the void ratio but also the suction or the degree of saturation, in which the suction and the degree of saturation are controlled or measured variables in laboratory testing. In general, for unsaturated soils, the ultimate deviator stress increases with the increases of confining pressure and suction, and the volumetric strain changes during shearing from contractive to dilative as confining pressure decreases and suction increases.

On the basis of the above experimental phenomena, it is concluded that the variation trends of the ultimate deviator stress with confining pressure and suction are consistent, which could be captured by the formulation of effective stress of unsaturated soil, i.e., average soil skeleton stress proposed by Bishop (1959). The contribution of the difference between pore air pressure and pore water pressure to strength was well considered in the effective stress for unsaturated soil. However, the variation trends of the volumetric strain during shearing with confining pressure and suction are opposite, which could not be captured by the average soil skeleton stress. The suction or, to be more precise, the unsaturated state affects the mechanical behaviour of unsaturated soils in two different ways (Jommi 2000; Gallipoli et al. 2003): (a) increasing the skeleton stress due to the equivalent pore pressure acting in the soil pores; (b) providing an additional "bonding" generated by water menisci at the particle contacts due to capillary phenomena. As a result of the additional "bonding" to the particle contacts, the critical state lines (CSLs) under saturated and unsaturated states are not unique in e-log$p$' (void ratio - mean effective stress) plane even through the Bishop stress is chosen as a stress variable. In other words, the value of void ratio at critical state of unsaturated soil is always greater than that under saturated condition under the same value of mean effective stress. Thus the "bonding" phenomenon influences the density state of the soil (e.g., e_c/e or e-e_c where e_c is the critical void ratio corresponding to the same mean average soil skeleton stress) and controls the contractive/dilative behaviour.

Normally suction is a controllable and independent variable in conventional laboratory tests for unsaturated soils. Choosing suction as an addition variable is convenient. Thus, the variations of intercept and slope for the compression lines with suction were widely discussed. On the other hand, the soil compression index was assumed to be a function of the degree of saturation for unsaturated soils by Zhang and Ikariya (2011) and Zhou et al. (2012a). Moreover, the intercept of the critical state lines in the e-logp' plane under unsaturated state was also assumed to be a function of the degree of saturation by Zhang and Ikariya (2011). Zhang and Ikariya (2011) assumed that the intercepts of the normal consolidation lines and the critical state lines change linearly with the degree of saturation, and their slopes are constant. Zhou et al. (2012a) assumed that the change of slopes for the normal consolidation lines with the degree of saturation follows the power function equation, and their intercepts are constant.

Wheeler et al. (2003) demonstrated that the additional "bonding" force due to meniscus water lens could be well depicted by the degree of saturation rather than suction. Although further experimental evidence is needed to assess the rationality of choosing degree of saturation as state variable to replace suction (Burton et al. 2016), the bonding effect on the void ratios under compression state and critical state could be taken into account by introducing the effective degree of saturation.

The constitutive modelling considering contraction/dilatancy of unsaturated geo-materials could be fallen into two categories, i.e., Cam-Clay type models (e.g., Alonso et al. 1990; Gallipoli et al. 2003; Wheeler et al. 2003; Sheng et al. 2004; Tamagnini 2004; Li 2007; Sun 2008; Zhang and Ikariya 2011; Zhou et al. 2012b; Yao et al. 2014; Hu et al. 2015; Zhou and Sheng 2015; Ma et al. 2016; Ghasemzadeh et al. 2017; Li et al. 2017; Li and Yang 2018) and multi-mechanism models (Chiu and Ng 2003):

(a) In Cam-Clay type models, conventionally, the location of the CSL in the e-logp_{net} (void ratio - mean net stress) plane or in the e-logp' (void ratio - mean effective stress) plane is implicitly governed by the intersection point of the yield surface with the CSL in the p''-q plane where p'' represents p_{net} or p' and is consistent with the chosen constitutive stress variable of constitutive modelling. As a result, the contractive and dilative volumetric change during shearing could not be accurately captured. Otherwise, a very complex yield function with additional parameters (Zhang and Ikariya 2011; Li and Yang 2018) needs to be formulated if the location of the CSL in the e-logp'' plane is regarded as starting point, which still has the problem of predictive performance and potentially numerical convergence.

(b) In the multi-mechanism model proposed by Chiu and Ng (2003), a state-dependent dilatancy formulation is introduced to account for the effects of stress level and soil suction. The locations of CSLs under saturated and unsaturated states in the e-logp_{net} plane can be explicitly adopted, which guarantees the simulation of the contractive and dilative volumetric changes up to critical states.

Owing to the framework of Cam-Clay model, the first category of models is appropriate for soil with normal consolidated and slightly over-consolidated soils rather than over-consolidated soils. The prediction ability of second category of models for the contractive and dilative behaviours would be generally better than the first category of models due to the explicitly expression of CSL. Besides, using the average soil skeleton stress and suction as constitutive variables, several constitutive models for unsaturated soils were proposed considering the coupling of mechanical and hydraulic behaviours (e.g., Wheeler et al. 2003; Sheng et al. 2004; Tamagnini 2004; Li 2007; Sun et al. 2007, 2010; Sun et al. 2012; Li et al. 2017).

This paper presents a novel elasto-plastic model for unsaturated soils on the basis of the double-yield-surface model and combined with an explicit effective degree of saturation dependent location of the critical state line in e-logp' plane. It takes into account two plastic deformation mechanisms, i.e., compression and shear sliding, for unsaturated soils, which is established based on the critical state concept. The model performance is finally examined by comparing experimental results and simulations of triaxial tests on different unsaturated soils: silty sand, Speswhite kaolin and Jossigny silty clay.

Constitutive model

In this paper, the average soil skeleton stress is chosen as a constitutive stress to establish the mechanical model. Besides, the effective degree of saturation and the void ratio are chosen as state variables for the mechanical model.

The average soil skeleton stress considers the effect of suction *s*, and reads:

$$\sigma'_{ij} = \sigma_{ij,net} - sS_{re}\delta_{ij} \tag{1}$$

where $\sigma_{ij,net}$ is the net stress tensor, s is the suction, S_{re} is the effective degree of saturation and δ_{ij} is the Kronecher's delta.

Alonso et al. (2010), Lu et al. (2010) and Mašín (2013) stated that experimental data on stiffness and shear strength of unsaturated soil implies that the proportion of suction contributing to the effective stress is often overestimated, especially for high-plasticity clay, if the term 'suction times degree of saturation' is used in effective stress expressions of the Bishop type. It is suggested that the degree of saturation should be replaced by the effective saturation to eliminate the overestimated effect, where the effective degree of saturation is related to the amount of free water partially filled in the macropores.

In Eq.(1), the effective degree of saturation is chosen as the effective stress parameter to accurately determine the value of interparticle stress and adopted to describe the bonding effect, as follows:

$$S_{re} = \frac{S_r - S_{rres}}{1 - S_{rres}} \tag{2}$$

where S_{rres} is the residual degree of saturation, which defines the amount of water that remains primarily in the form of thin liquid films on solid particles but has very slight effect on suction stress as a part of average soil skeleton stress (Lu et al. 2010). In fact, the quantity of adsorbed water is not constant, which decreases after an initial increase with decreasing suction (Christenson 1994; Tuller et al. 1999; Baker and Frydman 2009). The adsorbed water retention curve considering the effect of suction and capillary condensation was established by Tuller and Or (2005), Konrad and Lebeau (2015) and Zhou et al. (2016). In order to simplify and put emphasis on the proposed mechanical constitutive framework, the residual degree of saturation was assumed to be a constant.

Elastic behaviour

The elastic behaviour of the deformation is assumed to be isotropic:

$$\mathrm{d}\varepsilon_{ij}^{e} = \frac{1+\upsilon}{E}\mathrm{d}\sigma'_{ij} - \frac{\upsilon}{E}\mathrm{d}\sigma'_{kk}\delta_{ij} \tag{3}$$

where υ is the Poisson's ratio which value could be assumed to be equal to 0.3 for soils; E is the Young's modulus which can be replaced by the elastic bulk modulus K through $E = 3K(1-2\upsilon)$; the elastic bulk modulus K is determined by the relation $K = p'(1+e_0)/\kappa$ with the slope of the swelling line κ in e-lnp' plane and the initial void ratio e_0.

Plastic behaviour

Two plastic criteria are introduced to represent the irreversible mechanical behaviour of unsaturated soil, which are the compression and shear-sliding criteria, respectively.

Compression criterion

For elastoplastic models, the transition between pure elastic strain and plastic strain is sudden during loading path. To depict the smooth plastic deformation from pure elastic state to compression criterion being active or from only shear-sliding criterion being active to both criteria being active, the bounding surface theory was adopted for compression criterion. Therefore, a bounding surface f_c^b and a loading surface corresponding to the current stress state f_c^c are defined, shown in Figure 1(a). Their expressions are

$$f_c^b = \overline{p}'^2 + \frac{3}{2}\frac{\overline{s}_{ij}\overline{s}_{ij}}{R^2} - p_c'^{b2} \tag{4}$$

$$f_c^c = p'^2 + \frac{3}{2}\frac{s_{ij}s_{ij}}{R^2} - p_c'^{c2} \tag{5}$$

where the stress point $\overline{\sigma}'_{ij}$ lies on the compression bounding surface and is defined according to a radial mapping rule so that it has the same stress ratio as the current stress point, defined by $\eta = \overline{q}/\overline{p}' = q/p'$; p' and q are mean average soil skeleton stress and deviator stress, respectively; s_{ij} is deviator stress tensor and defined by $s_{ij} = \sigma'_{ij} - p'\delta_{ij}$; R is a material parameter controlling the ratio of the long axis and the minor axis of ellipse; $p_c'^b$ and $p_c'^c$ are the hardening parameters controlling the size of the compression bounding surface and the compression current stress surface.

The compression yield surface is usually adopted for the multi-mechanism models to describe the compressible behaviour of saturated clay. For unsaturated clays, however, the irreversible contractive volumetric strain under isotropic stress state is attributed not only to the compression caused by the increase of mean average soil skeleton stress, but also to the collapse caused by the wetting which could be depicted by the loading-collapse (LC) yield curve. The LC yield curve is the right intersection line of the compression bounding surface with the $q = 0$ plane, which represents the variation of $p_c'^b$ with suction (Alonso et al. 1990; Sheng et al. 2004; Sun et al. 2008) or other variables, such as degree of saturation (Wheeler et al. 2003; Tamagnini 2004; Zhou et al. 2012b), and the combination of suction and degree of saturation (Li 2007; Ma et al. 2016). The pore collapse will occur when the stress state reaches the LC yield curve during wetting. Two kinds of methods for obtaining the expression of the LC yield curve were usually adopted in literature. In the first one, the LC yield curve is indirectly determined by the expressions of the normal consolidation line at different unsaturated states, which leads to the dependency of the LC yield function on the intercepts and slopes of the normal consolidation line (Alonso et al. 1990; Sheng et al. 2004; Sun et al. 2008; Zhou et al. 2012b). In the second one, the expression of the LC yield curve is directly defined according to the effect mechanisms of the suction or the other variables on $p_c'^b$ (Wheeler et al. 2003; Tamagnini 2004; Li 2007; Ma et al. 2016).

Adopting the simplified method proposed by Wheeler et al. (2003), the hardening parameter $p_c'^b$ is assumed to be dependent on the number of meniscus water lenses of the contact between soil particle, which could be represented by the value of degree of saturation, or to be more exact the effective degree of saturation, rather than the suction. Therefore, the LC yield curve is a straight vertical line in the *s*-*p*' plane, as shown in Figure 1(b), where the thermodynamically proved modified suction proposed by Houlsby (1997) is substituted by the suction that most experimental data used. The modified suction is defined by the product of suction and porosity, which is conjugated to the increment of effective degree of saturation.

Besides, the collapse behaviour upon wetting could be modelled by adopting a double-hardening law for the evolution of $p_c'^b$ (Wheeler et al., 2003). In the double-hardening law, the evolution of $p_c'^b$ is dependent not only on the plastic volumetric strain increment but also on the plastic increment of effective degree of saturation:

$$\frac{\mathrm{d}p_c'^b}{p_c'^b} = \frac{1+e_0}{\lambda-\kappa}\mathrm{d}\varepsilon_{v(c)}^p - b_{sw}\frac{\mathrm{d}S_{re}^p}{\lambda_w-\kappa_w} \tag{6}$$

and the evolution of $p_c'^c$ is expressed by

$$\frac{\mathrm{d}p_c'^c}{p_c'^c} = \frac{1}{\Omega}\frac{1+e_0}{\lambda-\kappa}\mathrm{d}\varepsilon_{v(c)}^p - b_{sw}\frac{\mathrm{d}S_{re}^p}{\lambda_w-\kappa_w} \tag{7}$$

where $\varepsilon_{v(c)}^p$ is the plastic volumetric strain caused by the compression criterion; λ is the slope of the normal consolidation line in the *e*-ln*p'* plane at saturated state; Ω is a scaling function controlling the hardening rate of the compression current stress surface, and defined by a simple expression $\Omega = (p_c'^b / p_c'^c)^4$; κ_w and λ_w are the slopes of the scanning lines and the primary drying or wetting line of the soil water retention curve; b_{sw} is the coupling parameter; $\mathrm{d}S_{re}^p$ is the plastic increment of effective degree of saturation.

Shear-sliding criterion

The shear-sliding yield surface is used to describe the shear sliding among soil particles. As the model for saturated soils (Yin et al. 2013a), a linear shear-sliding yield surface is adopted in $p'-q$ plane, as shown in Figure 1(a). The effect of suction on the expression of shear-sliding yield surface is considered by the equivalent pore pressure. Then, the expression of the shear-sliding yield surface is given by:

$$f_s = \sqrt{\frac{3}{2} r_{ij} r_{ij}} - H \tag{8}$$

where $r_{ij} = s_{ij} / p'$; H is the hardening parameter.

The hardening parameter H is defined by a hyperbolic function in $H - \varepsilon_d^p$ plane:

$$H = \frac{M_p \varepsilon_{d(s)}^p}{1/G_p + \varepsilon_{d(s)}^p} \tag{9}$$

where $\varepsilon_{d(s)}^p$ is the plastic shear strain caused by the shear-sliding criterion; G_p and M_p are soil parameters. As listed in Eq. (9), the hardening parameter H only varies with the plastic shear strain obeying the shear-sliding criterion, which ensures that the target void ratio of critical state could be reached at the situation of simultaneous yielding on compression and shear-sliding criterions. G_p controls the initial slope of the hyperbolic curve in the $\eta' - \varepsilon_d^p$ plane. M_p represents the peak stress ratio related to the peak friction angle ϕ_p by $M_p = 6\sin\phi_p / (3 - \sin\phi_p)$ in triaxial compression for instance. Note that three-dimensional strength criteria can be introduced by different ways (Yao et al., 2004, 2008). Yin et al. (2013b) proposed that the shear modulus is related to the over-consolidation ratio (OCR) to consider the hardening effects and could be expressed by

$$G_p = G_{p0}\left(\frac{p_c'^{b}}{p_c'^{c}}\right)^{n_G} \tag{10}$$

where G_{p0} is a soil parameter; parameter n_G controls the variation ratio of G_p with OCR, and the value of n_G could be assumed equal to 1 for simplicity.

Furthermore, according to Jin et al. (2016, 2018), the value of the peak friction angle ϕ_p is linked to the internal friction angle ϕ_μ and the soil density state (e_c/e) by the following relation:

$$\tan\phi_p = \left(\frac{e_c}{e}\right)^{n_p}\tan\phi_\mu \tag{11}$$

where parameter n_p controls the variation ratio of $\tan\phi_p$ with the soil density state (e_c/e). The critical void ratio e_c is the void ratio at the CSL with the same average soil skeleton stress of the current void ratio in $e-\ln p'$ plane.

Because of the bonding effect provided by the air-water interface, the CSLs in $e-\ln p'$ plane do not coincide with each other at unsaturated state. Then, a group of parallel CSLs at different effective degree of saturation could be defined by (Zhang and Ikariya 2011):

$$\begin{aligned} &e_c = \Gamma_c - \lambda_c \ln p' \quad \text{with} \\ &\Gamma_c(S_{re}) = \Gamma_{csat} - a_\Gamma S_{re}, \quad \lambda_c = \text{constant} \end{aligned} \tag{12}$$

where $\Gamma_c(S_{re})$ and λ_c are respectively the intercept and slope of CSL in $(e-\ln p')$ plane with λ_c assumed equal to λ for simplicity; Γ_{csat} is the intercept of critical state line at saturated state in $e-\ln p'$ plane; a_Γ is model parameters; $a_\Gamma S_{re}$ represents the influence of suction bonding on the critical state. The linear variation of the intercept of critical state line with the effective degree of saturation was adopted by Zhang and Ikariya (2011), which could be further confirmed by the triaxial tests results on compacted Speswhite kaolin by Sivakumar (1993) and on Jossigny silty clay by Cui and Delage (1996), as shown in Figure 2. The effective degree of saturations are determined by the Eq. (2), and the values of residual degree of saturation are presented in Table 1.

In order to take into account the dilation or contraction during shear sliding, a non-associated flow rule is introduced, and an explicit derivation of the potential surface g_s is given by:

$$\begin{aligned}&\frac{\partial g_s}{\partial \sigma'_{ij}}=\frac{\partial g}{\partial p'}\frac{\partial p'}{\partial \sigma'_{ij}}+\frac{\partial g}{\partial s_{ij}}\frac{\partial s_{ij}}{\partial \sigma'_{ij}} \quad \text{with}\\ &\frac{\partial g_s}{\partial p'}=D\left(M_{pt}-\sqrt{\frac{3}{2}r_{ij}r_{ij}}\right); \quad \frac{\partial g_s}{\partial s_{ij}}=\sqrt{\frac{3}{2}}\frac{r_{ij}}{\sqrt{r_{ij}r_{ij}}}\end{aligned} \tag{13}$$

where D and M_{pt} are soil parameters. D is a soil constant controlling the magnitude of dilatancy. M_{pt} is the slope of the phase transformation line which depends on the phase transformation angle ϕ_{pt} by $M_{pt}=6\sin\phi_{pt}/(3-\sin\phi_{pt})$ in triaxial compression for instance. Like the expression of ϕ_p, the value of ϕ_{pt} is also dependent on ϕ_μ and (e_c/e) (Yin et al., 2016, 2017):

$$\tan\phi_{pt} = \left(\frac{e_c}{e}\right)^{-n_{pt}} \tan\phi_\mu \quad (14)$$

where parameter n_{pt} controls the variation ratio of $\tan\phi_{pt}$ with the soil density state (e_c/e).

The peak friction angle ϕ_p and the phase transformation angle ϕ_{pt} are determined for the hardening parameter H and non-associated flow rule of shear-sliding criterion, respectively, which are varying with the soil density state (e_c/e). Eqs. (11) and (14) imply that for a dense structure, e is lower than e_c and $\phi_{pt} \le \phi_\mu \le \phi_p$ is satisfied under initial state. At the initial phase, $\eta = q/p'$ is lower than the initial value of M_{pt}. Therefore, the volumetric strain is first contractive according to Eq. (14). With the increasing of q, η becomes greater than M_{pt}, and thus the volumetric strain is dilative according to Eq. (14) with e increasing. M_{pt} and M_p is fully related to (e_c/e). With the increasing of e, the difference among M_{pt}, M_p and M is gradual eliminated. When e is equal to e_c, the value of M_{pt}, M_p and M are the same. Then at the critical state, the volumetric strain is a constant according to Eq. (14). On the other hands, for a loose structure, e is greater than e_c and $\phi_{pt} \ge \phi_\mu \ge \phi_p$ is satisfied under initial state. During shearing stage, η is lower than the initial value of M_{pt}, and thus the volumetric strain is contractive according to Eq. (14) with e decreasing. As a result, the difference among M_{pt}, M_p and M becomes slight. When e is equal to e_c, the values of M_{pt}, M_p and M are the same, and the volumetric strain becomes constant according to Eq. (14). The above analysis illustrated that Eqs. (9), (11), (13) and (14) guarantee stresses and void ratio reach simultaneously the critical state in the p'-q-e space.

Description of soil-water retention curve

The soil-water retention curve (SWRC) is usually adopted to describe the relationship between water content and suction, which represents the water retention behaviour for unsaturated soils. There are two important features of water retention behaviour for unsaturated soils, i.e., hydraulic hysteresis and density dependency. It means that the values of S_{re} can be significantly different for the samples with the same suction, which also depends on the hydraulic path and soil dry density. For a typical SWRC considering the hydraulic hysteresis, it consists of main wetting and drying curves and scanning lines as shown in Figure 3. An initial point A stated in the region limited by the main wetting and drying curves will first shift following a scanning line until reaching the main drying line at point B during drying or the main wetting line at point C during wetting. Elastic change of S_{re} occurs in this region, which corresponds to reversible movements of the air–water interfaces without draining or flooding of voids. Further drying or wetting will follow the main drying curve or the main wetting curve, which leads to elasto-plastic change of S_{re}. The elasto-plastic change of S_{re} corresponds to draining or flooding of voids with water. Moreover, to describe the density dependency, the position of SWRC in the s-S_{re} plane should be shift with the soil dry density. In general, the SWRC moves right with increasing dry density, and moves left with decreasing dry density, which implies that the values of S_{re} for a dense soil sample is higher than that for a loose one with the same s and hydraulic path. The models for soil-water retention behaviour were established for considering hydraulic hysteresis (e.g., Li 2005; Muraleetharan et al. 2009; Pedroso and Williams 2010), density dependency (e.g., Zhou et al. 2012c; Zhou et al, 2014; Tan et al. 2016) and both of them (e.g., Wheeler et al. 2003; Sheng and Zhou 2011; Tarantino 2015).

The elasto-plastic model is developed to describe the water retention behaviour with hydraulic hysteresis and density dependency of unsaturated soil. The approach is similar to that of Wheeler et al. (2003), expect for the modified suction replaced by the suction, the degree of saturation replaced by the effective saturation, and eliminating the restriction of values of coupling parameters. The character of hydraulic hysteresis is depicted by a group of yield surfaces, i.e., suction increasing yield surface and suction decreasing yield surface (f_{si} and f_{sd}). An elastic zone is bounded by the group of yield surfaces. During drying and wetting paths, elastic change of S_{re} occurs in this elastic region, and elasto-plastic change of S_{re} occurs when the suction increasing or decreasing yield surface actives. The suction increasing and decreasing yield surfaces, is defined by

$$\begin{cases} f_{si} = s - s_i & \text{for drying path} \\ f_{sd} = s_d - s & \text{for wetting path} \end{cases} \tag{15}$$

where s_i and s_d are hardening parameters, representing the intersections of scanning line with the main drying and wetting lines, respectively.

The total degree of saturation S_r could be decomposed by:

$$S_r = S_{re}(1 - S_{rres}) + S_{rres} \tag{16}$$

Since the residual degree of saturation is assumed to be a constant, the increment of total degree of saturation is only related to the increment of effective degree of saturation. The increment of effective degree of saturation is divided into elastic and plastic parts, and the elastic part is defined by

$$\mathrm{d}S_{re}^{e} = \kappa_w \frac{\mathrm{d}s}{s + p_a} \tag{17}$$

where κ_w is a constant and is the slope of scanning line in $\ln(s+p_a)$-S_{re} plane; p_a is a constant to avoid null denominator, and it is usually assumed equal to the atmospheric pressure for simplicity.

To consider the density dependency, the other double-hardening law is adopted for the evolutions of s_i and s_d. The hardening variables of s_i and s_d are varying not only with the plastic degree of saturation, but also with the plastic volumetric strain, which leads to an additional plastic change of S_{re}. The double-hardening law is thus expressed by

$$\begin{cases} \dfrac{\mathrm{d}s_i}{s_i + p_a} = \dfrac{1}{\lambda_w - \kappa_w}\mathrm{d}S_{re}^{p} + b_{ws}\dfrac{1+e_0}{\lambda - \kappa}\mathrm{d}\varepsilon_v^{p} \\ \dfrac{\mathrm{d}s_d}{s_d + p_a} = \dfrac{1}{\lambda_w - \kappa_w}\mathrm{d}S_{re}^{p} + b_{ws}\dfrac{1+e_0}{\lambda - \kappa}\mathrm{d}\varepsilon_v^{p} \end{cases} \tag{18}$$

where λ_w is the slope of main drying or wetting curve in $\ln(s+p_a)$-S_{re} plane, which value can be assumed constant or determined by the expression of the main drying or wetting curve; b_{ws} is the another coupling parameter. As shown in Figure 1(b), the bounding surface f_c^b intersects with f_{si} and f_{sd} yield surfaces. Therefore, there are four possible outcomes when the stress state is at the corner depending on the stress path direction, which are elastic unloading, yielding on the f_{si} (or f_{sd}) only, yielding on the f_c^b curve only, or simultaneous yielding. To avoid numerical failure of the model when the stress state reaches one of these corners, a restriction on the values of the coupling parameters, i.e., $b_{sw}b_{ws} < 1$ was proposed by Wheeler et al. (2003) according to the situation of simultaneous yielding on the f_{si} (or f_{sd}) and f_c^b curves. In fact, there is no denying that this restriction is improper for the other two plastic situations, i.e., yielding on the f_{si} (or f_{sd}) only and yielding on the f_c^b curve only. That is to say, the above restriction does not follow the fact. Therefore, different from Wheeler et al. (2003) this restriction is not adopted in this proposed model, and the success of the model when the stress state reaches any one of these corners could be guaranteed using the stress integration algorithm with clear distinction of four cases.

Applying the consistency conditions for the compression, shear-sliding and suction increasing (or decreasing) yield surfaces and combining the elastic constitutive equations (3) and (17), the incremental general stress–strain equations can be obtained.

The ability of an elasto-plastic model under isotropic stress state with the double hardening laws were verified by Wheeler et al. (2013). The verification could be extended to the proposed bounding surface model: (i) During drying, the average soil skeleton stress increases with the increasing of suction, as shown in Figure 4(a). The irreversible compression will occur due to the fact that the average soil skeleton approaches the loading-collapse bounding surface during drying path. The loading-collapse bounding surface moves right due to the increasing of plastic volumetric strain. Besides, according to the double hardening laws, the suctions increasing and decreasing yield surfaces will shift upward when the plastic volumetric strain occurs. Therefore, the plastic degree of saturation is not zero when their loading criterions are satisfied due to the variations of suction or hardening parameters. (ii) During wetting, the average soil skeleton stress decreases with the decreasing of suction, as shown in Figure 4(b). The plastic degree of saturation will increase when the suction reaches the suction decreasing yield surfaces. According to the double hardening laws, the loading-collapse bounding surface moves left with the increasing of plastic degree of saturation. When the reduction of $p_c'^b$ larger than p', the average soil skeleton virtually approaches the loading-collapse bounding surface during wetting path, which leads to the collapse during wetting.

Model parameters

The model contains 15 material parameters, which can be divided into three groups, i.e., related to the compression criterion (λ, κ, b_{sw}), related to the shear-sliding criterion (ϕ_μ, G_{p0}, n_p, Γ_{csat}, a_Γ, D, n_{pt}), and related to the SWRC (λ_w, κ_w, p_a, b_{ws}, S_{rres}). The determination of the model parameters is summarized below.

The slopes of the normal consolidation line λ and the swelling line κ can be determined from an isotropic compression test on saturated sample. The coupling parameter b_{sw} can be calibrated from the isotropic compression tests on unsaturated samples.

The internal friction angle ϕ_μ can be obtained from M_c by $M_c = 6\sin\phi_\mu / (3-\sin\phi_\mu)$ which is the slope of the critical state line in $p'-q$ plane under triaxial compression. Then the parameters related to the CSLs in $p'-q$ plane (ϕ_μ) and in $e-\ln p'$ plane (Γ_{csat} and a_Γ) can be determined by triaxial tests up to failure at unsaturated state.

The plastic stiffness G_{p0} can be obtained by curve fitting from the deviatoric stress-strain curve at small strain level in saturated or unsaturated states. Parameter n_p can be obtained by curve fitting from the evolution of deviatoric stress-strain during a drained test. The dilatancy constant D and parameter n_{pt} can be determined by curve fitting from the evolution of the volumetric strain during a drained test.

For the sake of simplicity, the variation of effective degree of saturation S_{re} with the main wetting and drying lines is assumed to be linear with the logarithmic value of $(s+p_a)$ (Wheeler et al. 2003; Sun et al. 2007; Li et al. 2017). Then the slope of the primary wetting and drying lines of SWRC λ_w and the slope of the scanning line κ_w in the $S_{re}-\ln(s+p_a)$ plane are assumed constant and can be determined from soil water retention tests by the pressure plate method, filter paper method or vapour equilibrium technique where the volumetric strain should be controlled or measured. The gradient b_{ws} can be calibrated from a consolidation compression under constant suction. The value of the residual degree of saturation S_{rres} can be obtained to guarantee that the critical state lines in the *p'*-*q* plane under saturated and unsaturated state are coincides each other according to the method proposed by Alonso et al. (2010) and Oh and Lu (2014).

Note that, alternatively all parameters can also be identified by using optimization methods based on necessary experimental data relating to different groups of parameters (Jin et al., 2017; Yin et al., 2018).

For the proposed mechanical model, the skeleton stress is chosen as a constitutive stress, and the effective degree of saturation and the void ratio are chosen as state variables. The skeleton stress considers the contribution of the equivalent pore pressure acting in the soil pores, and the effective degree of saturation considers the contribution of the additional "bonding" to the particle contacts. The model took into account the two plastic deformation mechanisms, i.e. compression and shear sliding. The skeleton stress is used for the compression and shear-sliding ones, and the hardening law for the compression one and the critical state lines for the shear-sliding one consider the effect of additional "bonding". Combined with non-associated flow rule for the shear sliding mechanism, the S_{re}-dependence of critical state line in the e-logp' plane guarantees (a) the contractive and dilative shear behaviours for unsaturated soils during shear stage and (b) stresses and void ratio reach simultaneously the critical state in the p'-q-e space, which could be verified by simulating triaxial tests of unsaturated soil.

Test simulation and model validation

Three series of drained triaxial tests on unsaturated soils were selected for the model's validation. The first series was carried out on compacted silty sand by Rampino et al. (2000). The second series was carried out on compacted Speswhite kaolin by Sivakumar (1993). The third series was carried out on compacted Jossigny silty clay by Cui and Delage (1996). All the parameters used in the subsequent simulations were determined according to section 2.4. The values of the material and initial state parameters are summarized in Table 1.

Silty sand

Drained triaxial tests were carried out on compacted silty sand by Rampino et al. (2000). The soil was mixed by finer and coarser grained soils to achieve the in situ uniformity coefficient C_u of 400. The specimens were first wetted to obtain different suctions (300, 200 and 100 kPa) under a mean net stress of 10 kPa, and then they were consolidated under mean stresses of 100 and 400 kPa at different suctions. Finally, all soil specimens were sheared under drained condition at constant net confining stress and constant suction. The suctions of Samples No. 5, 7, 10, 14 were 100, 200, 200 and 300 kPa, respectively and the corresponding constant net confining stresses were 400, 100, 400 and 400 kPa, respectively.

Figure 5 shows the variations of the deviatoric stress, the specific volume and the degree of saturation during the triaxial tests. The comparison between the measured and calculated results shows that the model can satisfactorily reproduce the shear-dilative behaviour of unsaturated silty sand under different suctions and net confining stresses. The initial void ratio is lower than the critical void ratio corresponding to the same mean average soil skeleton stress for each sample. Therefore, all of them first contract and then expand during deviatoric loading. Because the water retention behaviour is dependent of density, the degree of saturation of each specimen first decreases and then increases with the axial strain under constant suction, which trend is consistent with the volumetric strain change. For Sample No. 14, the test result of degree of saturation was not listed in the literature. Therefore, only calculated result is shown in Figure 5.

Speswhite kaolin

Drained triaxial tests were carried out on compacted Speswhite kaolin by Sivakumar (1993). The clay fraction is 75%. The specimens were first wetted to obtain different suctions (300, 200 and 100 kPa) under a mean net stress of 50 kPa, and then they were consolidated under mean stresses of 100 and 150 kPa at different suctions. Finally, all soil specimens were sheared under drained condition at constant net confining stress and constant suction. The suctions of Samples 8c, 9c, 13c, 17c and 18c were 200, 200, 100, 300 and 300 kPa, respectively and the corresponding constant net confining stresses were 150, 100, 100, 100 and 150 kPa, respectively.

Figure 6 shows the variations of the deviatoric stress, the specific volume and the degree of saturation during the triaxial tests. The comparison between the measured and calculated results shows that the model can satisfactorily reproduce the shearing behaviour of unsaturated soil under different suctions and net confining stresses. Because the initial void ratio is higher than the critical void ratio corresponding to the same mean average soil skeleton stress for each sample, all of samples experience a continuous strain hardening. Besides, the degree of saturation of each specimen increases with the axial strain under constant suction due to the contractive volumetric strain. It should be noted that the completed triaxial test consists of compression and shear stages. Both of them are simulated by the proposed model. Lack of test results during compression stage, the comparison between calculated and measured results during compression stage is not illustrated.

Jossigny silty clay

Drained triaxial tests were carried out on compacted Jossigny silty clay by Cui and Delage (1996). The clay minerals are illite, kaolinite and inter-stratified illite-smectite. The osmotic technique was used to control the suction during triaxial compression tests. The specimens were first dried to different targeted suctions (200, 400, 800 and 1500 kPa) under zero applied stress, and then consolidated under different mean net stresses of 50, 100, 200, 400 and 600 kPa at different suctions. Finally, all the soil specimens were sheared under drained condition at constant net confining stress and constant suction.

Figures 7 to 10 show the evolution of the deviatoric stress and volumetric strain during the triaxial tests. The comparison between measured and calculated results shows that the model can satisfactorily reproduce the contraction and dilation during shearing because of the adopted non-associated flow rule for the shear-sliding yield surface. For saturation soil, dilatancy will occurs when the confining stress is lower than a threshold value. The threshold value increases with increasing suction for unsaturated soil. It means that the suction, specifically, the additional “bonding” generated by water menisci enhanced the shear-dilative behaviour. All these simulated results are in agreement with the experimental data. Besides, the shear strength increases with the net confining stress and the suction, and the final value of the specific volume varies with the net confining stress and the suction. Due to the lack of measured values of degree of saturation during triaxial compression, the comparison between calculated and measured degrees of saturation is not possible. The variation trend of degree of saturation for Jossigny silty clay is similar with that for Silty sand and Speswhite kaolin during shear stage, which increases with the increasing of axial strain. Furthermore, compared to Zhang and Ikariya (2011) the proposed model achieved a better prediction performance.

Overall, the general trends of mechanical behavior for unsaturated soils were well captured by the proposed model. However, the accuracy of prediction for all above three soils still needs to be improved, especially for the third series of drained triaxial tests for Jossigny silty clay. The predictive ability of the proposed model could be improved if S_{re}-dependence of parameters related to the shear-sliding criterion (e.g., n_p, D, n_{pt}) are formulated. However, these additional functions will induce mathematic complexity with more input parameters, which would limit the practicability of the proposed model. Furthermore, the unsaturated soil samples are not always identical, and the osmotic technique controlled the suction is not easy to carry out. Therefore, the randomness of sample and test result should be paid attention to, which was not included in the model and simulations.

Conclusions

A critical state based elasto-plastic model with two plastic deformation mechanisms has been developed for unsaturated soils. Firstly, the average soil skeleton stress was chosen as a constitutive stress, and the effective degree of saturation and the void ratio were chosen as state variables for the mechanical model. The effective degree of saturation was substituted for the degree of saturation to eliminate the overestimation for proportion of suction contributing to the effective stress.

Secondly, the explicit CSL expression makes the relationship between the critical state line and the normal consolidation line more flexible than that under the framework of the Cam-Clay models. This formulation of CSL with the non-associated flow rule for the shear sliding yield surface guarantees that the proposed model can well reproduce the dilation or contraction during shear for unsaturated soils.

Thirdly, the coupling between mechanical and water retention behaviours is considered by the double hardening law, where the restriction on the values of the coupling parameters, i.e., $b_{sw}b_{ws} < 1$ is not adopted, and the success of the model when the stress state reaches any one of these corners could be guaranteed using the stress integration algorithm with clear distinction of four cases.

Finally, the predictive ability of the model to reproduce the mechanical behaviours during shear stage of unsaturated soil was analysed by comparing the numerical simulations and the experimental data from the triaxial tests on silty sand, Speswhite kaolin and Jossigny silty clay. All comparisons have demonstrated that the proposed model can reproduce, with good accuracy, the shear strength and the dilative and contractive behaviour of unsaturated soils.

Acknowledgments

This research was financially supported by the National Natural Science Foundation of China (Grant No. 51579179); a RIF project (Grant No.: PolyU R5037-18F) from Research Grants

Council (RGC) of Hong Kong Special Administrative Region Government (HKSARG) of China; the National State Key Project "973" grant [grant number 2014 CB047000, sub-project grant number 2014 CB047001] from Ministry of Science and Technology of the People's Republic of China; and the Research Funds of Henan Provincial Department of Transportation [grant number 2017B4].

References

Ajdari, M., Habibagahi, G., Nowamooz, H., Masrouri, F., and Ghahramani, A. 2010. Shear strength behaviour and soil water retention curve of a dual porosity silt-bentonite mixture. Scientia Iranica, Transaction A, Civil Engineering, **17**(6): 430-440. doi: doi:10.1680/wama.900024.

Alonso, E.E., Gens, A., and Josa, A. 1990. A constitutive model for partially saturated soils. Géotechnique, **40**(3): 405-430. doi:10.1680/geot.1990.40.3.405.

Alonso, E.E., Pereira, J.-M., Vaunat, J., and Olivella, S. 2010. A microstructurally based effective stress for unsaturated soils. Géotechnique, **60**(12): 913-925. doi:10.1680/geot.8.P.002.

Baker, R., and Frydman, S. 2009. Unsaturated soil mechanics: Critical review of physical foundations. Engineering Geology, **106**(1-2): 26-39. doi:10.1016/j.enggeo.2009.02.010.

Bishop, A.W. 1959. The principle of effective stress. Teknisk Ukeblad, **106**: 113-143.

Burton, G.J., Pineda, J.A., Sheng, D., Airey, D.W., and Zhang F. 2016. Exploring one-dimensional compression of compacted clay under constant degree of saturation paths. Géotechnique, **66**(5): 435-440 doi:10.1680/jgeot.14.P.181.

Cattoni, E., Cecconi, M., and Jommi, C. 2005. Soil dilatancy and suction: some remarks on their mutual effects on the shear strength of granular soils. *In* Proceedings of the 11th

International Conference on Computers Methods and Advances in Geomechanics, Torino, Italy. pp. 19-26.

Chiu, C.F., and Ng, C.W.W. 2003. A state-dependent elasto-plastic model for saturated and unsaturated soils. Géotechnique, **53**(9): 809-829. doi:10.1680/geot.2003.53.9.809.

Christenson, H.K. 1994. Capillary condensation due to van der Waals attraction in wet slits. Physical Review Letters, **73**(13): 1821-1824. doi: 10.1103/PhysRevLett. 73.1821.

Cui, Y.J., and Delage, P. 1996. Yielding and plastic behaviour of an unsaturated compacted silt. Géotechnique, **46**(2): 291-311. doi:10.1680/geot.1996.46.2.291.

Cui, Q.L., Shen, S.L., Xu, Y.S., Wu, H.N., and Yin, Z.-Y. 2015. Mitigation of geohazards during deep excavations in karst regions with caverns: a case study. Engineering Geology, **195**: 16-27. doi: 10.1016/j.enggeo.2015.05.024.

Estabragh, A.R., and Javadi, A.A. 2008. Critical state for overconsolidated unsaturated silty soil. Canadian Geotechnical Journal, **45**(3): 408-420. doi:10.1139/T07-105.

Estabragh, A.R., and Javadi, A.A. 2014. Roscoe and Hvorslev surfaces for unsaturated silty soil. International Journal of Geomechanics, **14**(2): 230-238. doi:10.1061/(ASCE)GM.1943-5622.0000306.

Fern, E.J., Robert, D.J., and Soga, K. 2016. Modeling the stress-dilatancy relationship of unsaturated silica sand in triaxial compression tests. Journal of Geotechnical and Geoenvironmental Engineering, **142**(11): 04016055. doi:10.1061/(ASCE)GT.1943-5606.0001546.

Futai, M.M., and Almelda, M.S.S. 2005. An experimental investigation of the mechanical behaviour of an unsaturated gneiss residual soil. Géotechnique, **55**(3): 201-213. doi:10.1680/geot.2005.55.3.201.

Gallipoli, D., Gens, A., Sharma, R., and Vaunat, J. 2003. An elasto-plastic model for unsaturated soil incorporating the effects of suction and degree of saturation on mechanical behaviour. Géotechnique, **53**(1): 123-135. doi:10.1680/geot.2003.53.1.123.

Ghasemzadeh, H., Sojoudi, M.H., Ghoreishian Amiri, S.A., and Karami, M.H. 2017. Elastoplastic model for hydro-mechanical behavior of unsaturated soils. Soils and

Foundations, **57**(3): 371-383. doi:10.1016/j.sandf.2017.05.005.

Houlsby, G., T. 1997. The work input to an unsaturated granular material. Géotechnique, **47**(1), 193-196. doi: 10.1680/geot.1997.47.1.193.

Hu, R., Chen, Y.F., Liu, H.H., and Zhou, C.B. 2015. A coupled stress-strain and hydraulic hysteresis model for unsaturated soils: thermodynamic analysis and model evaluation. Computers and Geotechnics, **63**: 159-170. doi:10.1016/j.compgeo.2014.09.006.

Huat, B.B.K., Ali, F.H., and Low, T.H. 2006. Water infiltration characteristics of unsaturated soil slope and its effect on suction and stability. Geotechnical and Geological Engineering, **24**(5), 1293-1306. doi: 10.1007/s10706-005-1881-8.

Jin, Y.-F., Yin, Z.-Y., Shen, S.L., and Hicher, P.Y. 2016. Selection of sand models and identification of parameters using an enhanced genetic algorithm. International Journal for Numerical and Analytical Methods in Geomechanics, **40**(8): 1219-1240. doi: 10.1002/nag.2487.

Jin, Y.-F., Yin, Z.-Y., Shen, S.L., and Zhang, D.M. 2017. A new hybrid real-coded genetic algorithm and its application to parameters identification of soils. Inverse Problems in Science and Engineering, **25**(9): 1343-1366. doi: 10.1080/17415977.2016.1259315.

Jin, Y.-F., Yin, Z.-Y., Wu, Z.-X., and Zhou, W.-H. 2018. Identifying parameters of easily crushable sand and application to offshore pile driving, Ocean Engineering, **154**: 416-429. doi: 10.1016/j.oceaneng.2018.01.023.

Jommi, C. 2000. Remarks on the constitutive modelling of unsaturated soils. *In* International Workshop on Unsaturated Soils: Experimental Evidence and Theoretical Approaches, Trento, Italy. *Edited by* A. Tarantino, C. Mancuso. pp. 139-153.

Kim, B.S., Park, S.W., Takeshita, Y., and Kato, S. 2016. Effect of suction stress on critical state of compacted silty soils under low confining pressure. International Journal of Geomechanics, **16**(6): D4016010. doi:10.1061/(ASCE)GM.1943-5622.0000665.

Konrad, J.-M., and Lebeau, M. 2015. Capillary-based effective stress formulation for predicting shear strength of unsaturated soils. Canadian Geotechnical Journal, **52**(12): 2067-2076. doi: 10.1139/cgj-2014-0300.

Li, J., Yin, Z.-Y., Cui, Y.J., and Hicher, P.-Y. 2017. Work input analysis for soils with double porosity and application to the hydro-mechanical modeling of unsaturated expansive clays. Canadian Geotechnical Journal, **54**(2): 173-187. doi: 10.1139/cgj-2015-0574.

Li, W., and Yang, Q. 2018. Hydromechanical constitutive model for unsaturated soils with different overconsolidation ratios. International Journal of Geomechanics, **18**(2), 04017142. doi:10.1061/(ASCE)GM.1943-5622.0001046.

Li, X.S. 2005. Modelling of hysteresis response for arbitrary wetting/drying paths. Computers and Geotechnics, **32**(2): 133-137. doi: 10.1016/j.compgeo.2004.12.002

Li, X.S. 2007. Thermodynamics-based constitutive framework for unsaturated soils. 2: A basic triaxial model. Géotechnique, **57**(5): 423-435. doi: 10.1680/geot.2007.57.5.423.

Lu, N., Godt, J.W., and Wu, D.T. 2010. A closed-form equation for effective stress in unsaturated soil. Water Resources Research, **46**(5): W05515. doi: 10.1029/2009WR008646

Lyu, H.M., Sun, W.J., Shen, S.L., and Arulrajah, A. 2018. Flood risk assessment in metro systems of mega-cities using a GIS-based modeling approach. Science of the Total Environment, **626**: 1012-1025. doi: 10.1016/j.scitotenv.2018.01.138.

Ma, T., Wei, C., Wei, H., and Li W. 2016. Hydraulic and mechanical behavior of unsaturated silt: Experimental and theoretical characterization. International Journal of Geomechanics, **16**(6): D4015007. doi: 10.1061/(ASCE)GM.1943-5622.0000576.

Mašín, D. 2013. Double structure hydromechanical coupling formalism and a model for unsaturated expansive clays. Engineering Geology, **165**, 73-88. doi: 10.1016/j.enggeo.2013.05.026.

Matsuoka, H., Sun, D.A., Kogane, A., Fukuzawa, N., and Ichihara, W. 2002. Stress-strain behaviour of unsaturated soil in true triaxial tests. Canadian Geotechnical Journal, **39**(3): 608-619. doi:10.1139/T02-031.

Muraleetharan, K.K., Liu, C., Wei, C., Kibbey, T.C.G., and Chen, L. 2009. An elastoplastic framework for coupling hydraulic and mechanical behavior of unsaturated soils. International Journal of Plasticity, **25**(3): 473-490. doi: 10.1016/j.ijplas.2008.04.001.

Ng, C.W.W., Sadeghi, H., and Jafarzadeh, F. 2016. Compression and shear strength characteristics of compacted loess at high suctions. Canadian Geotechnical Journal, **54**(5): 690-699. doi:10.1139/cgj-2016-0347.

Oh, S., and Lu, N. 2014. Uniqueness of the Suction Stress Characteristic Curve under Different Confining Stress Conditions. Vadose Zone Journal, **13**(5). doi:10.2136/vzj2013.04.0077.

Pedroso, D.M., and Williams, D.J. 2010. A novel approach for modelling soil-water characteristic curves with hysteresis. Computers and Geotechnics, **37**(3): 374-380. doi: 10.1016/j.compgeo.2009.12.004.

Pineda, J.A., and Colmenares, J.E. 2006. Stress-strain-suction behaviour of two clayey materials under unconfined conditions. *In* Proceedings of the 4th International Conference on Unsaturated Soils, UNSAT 2006, Arizona, USA. *Edited by* G.A. Miller, C.E. Zapata, S.L. Houston, and D.G. Fredlund. pp. 1109-1120. doi: 10.1061/40802(189)90.

Rampino, C., Mancuso, C., and Vinale, F. 2000. Experimental behaviour and modelling of an unsaturated compacted soil. Canadian Geotechnical Journal, **37**(4), 748-763. doi: 10.1139/t00-004.

Schofield A.N. 2006. Interlocking, and peak and design strengths. Géotechnique, **56**(5): 357-358. doi: 10.1680/geot.2006.56.5.357.

Schofield A.N. 2008. Discussion: Interlocking, and peak and design strengths. Géotechnique, **58**(6): 527-532. doi: 10.1680/geot.2008.D.006

Sheng, D., Sloan, S.W., and Gens, A. 2004. A constitutive model for unsaturated soils: thermomechanical and computational aspects. Computational Mechanics, **33**(6): 453-465. doi:10.1007/s00466-003-0545-x.

Sheng, D., and Zhou, A.N. 2011. Coupling hydraulic with mechanical models for unsaturated soils. Canadian Geotechnical Journal, **48**(5): 826-840. doi: 10.1139/t10-109.

Sivakumar, V. 1993. A critical state framework for unsaturated soil. Ph.D. thesis, University of Sheffield, Sheffield, UK.

Sun, D.A., Sheng, D., and Sloan S.W. 2007. Elastoplastic modelling of hydraulic and stress-strain behaviour of unsaturated soils. Mechanics of Materials, **39**(3), 212-221. doi: 10.1016/j.mechmat.2006.05.002.

Sun, D.A., Sheng, D., Xiang, L., and Sloan S.W. 2008. Elastoplastic prediction of hydro-mechanical behaviour of unsaturated soils under undrained conditions. Computers and Geotechnics, **35**(6): 845-852. doi:10.1016/j.compgeo.2008.08.002.

Sun, D.A., Sun, W.J., and Xiang, L. 2010. Effect of degree of saturation on mechanical behaviour of unsaturated soils and its elastoplastic simulation. Computers and Geotechnics, **37**(5), 678-688. doi: 10.1016/j.compgeo.2010.04.006.

Sun, W.J., and Sun, D.A. 2012. Coupled modelling of hydro-mechanical behaviour of unsaturated compacted expansive soils. International Journal for Numerical and Analytical Methods in Geomechanics, **36**(8), 1002-1022. doi: 10.1002/nag.1036.

Tamagnini, R. 2004. An extended Cam-clay model for unsaturated soils with hydraulic hysteresis. Géotechnique, **54**(3): 223-228. doi: 10.1680/geot.2004.54.3.223.

Tan, F., Zhou, W.H., and Yuen, K.V. 2016. Modeling the soil water retention properties of same-textured soils with different initial void ratios. Journal of Hydrology, **542**: 731-743. doi: 10.1016/j.jhydrol.2016.09.045.

Tang, M., Xu, Q., Huang, R. 2015. Site monitoring of suction and temporary pore water pressure in an ancient landslide in the three gorges reservoir area, China. Environmental Earth Sciences, 73(9), 5601-5609. doi: 10.1007/s12665-014-3814-4.

Tarantino, A. 2015. A water retention model for deformable soils. Géotechnique, **59**(9): 751-762. doi: 10.1680/geot.7.00118.

Thu, T.M., Rahardjo, H., and Leong, E.C. 2007. Critical state behaviour of a compacted silt specimen. Soils and foundations, **47**(4): 749-755. doi: 10.3208/sandf.47.749.

Tsai, T.L., Chen, H.E., and Yang, J.C. 2008. Numerical modeling of rainstorm-induced shallow landslides in saturated and unsaturated soils. Environmental Geology (Berlin), 55(6), 1269-1277. doi: 10.1007/s00254-007-1075-1.

Tuller, M., Or, D., and Dudley, L.M. 1999. Adsorption and capillary condensation in porous media: Liquid retention and interfacial configurations in angular pores. Water Resources Research, **35**(7): 1949-1964. doi: 10.1029/1999WR900098.

Tuller, M., and Or, D. 2005. Water films and scaling of soil characteristic curves at low water contents. Water Resources Research, **41**(9):W09403. doi: 0.1029/2005WR004142.

Vo, T., Russell, A.R. 2016. Bearing capacity of strip footings on unsaturated soils by the slip line theory. Computers and Geotechnics, **74**, 122-131. doi:10.1016/j.compgeo.2015.12.016.

Wheeler, S.J., Sharma, R.S., and Buisson, M.S.R. 2003. Coupling of hydraulic hysteresis and stress-strain behaviour in unsaturated soils. Géotechnique, **53**(1): 41-54. doi:10.1680/geot.2003.53.1.41.

Yao, Y., Sun, D., and Luo, T. 2004. A critical state model for sands dependent on stress and density. Int. J. Numer. Anal. Methods Geomech., **28**(4): 323–337.

Yao, Y., Sun, D., and Matsuoka, H. 2008. A unified constitutive model for both clay and sand with hardening parameter independent on stress path. Comput. Geotech., **35**(2): 210–222.

Yao, Y.P., Niu, L., and Cui, W.J. 2014. Unified hardening (UH) model for overconsolidated unsaturated soils. Canadian Geotechnical Journal, **51**(7): 810-821. doi: 10.1139/cgj-2013-0183.

Yin, Z.-Y., Xu, Q., and Hicher, P.-Y. 2013a. A simple critical-state-based double-yield-surface model for clay behaviour under complex loading. Acta Geotechnica, **8**(5): 509-523. doi:10.1007/s11440-013-0206-y.

Yin, Z.-Y., Xu, Q., and Chang, C.S. 2013b. Modeling cyclic behavior of clay by micromechanical approach. Journal of Engineering Mechanics ASCE, **139**(9): 1305-1309. doi: 10.1061/(asce)em.1943-7889.0000516

Yin, Z.-Y., Huang, H.W., and Hicher, P.Y. 2016. Elastoplastic modeling of sand-silt mixtures. Soils and Foundations,**56**(3): 520-532. doi: 10.1016/j.sandf.2016.04.017.

Yin, Z.-Y., Hicher, P.Y., Dano, C., and Jin, Y.F. 2017. Modeling the mechanical behavior of very coarse granular materials. Journal of Engineering Mechanics ASCE, **143**(1): C401600. doi: 10.1061/(ASCE)EM.1943-7889.0001059.

Yin, Z.-Y., Jin, Y.F., Shen, J.S., Hicher, P.Y. 2018. Optimization techniques for identifying soil parameters in geotechnical engineering: Comparative study and enhancement. International Journal for Numerical and Analytical Methods in Geomechanics, **42**(1):70-94. doi: 10.1002/nag.2714.

Zhan, T.L.T, and Ng, C.W.W. 2006. Shear strength characteristics of an unsaturated expansive clay. Canadian Geotechnical Journal, **43**(7): 751-763. doi: 10.1139/T06-036.

Zhang, F., and Ikariya, T. 2011. A new model for unsaturated soil using skeleton stress and degree of saturation as state variables. Soils and Foundations, **51**(1): 67-81. doi: 10.3208/sandf.51.67.

Zhou, A.-N., Sheng, D., Sloan, S.W., and Gens, A. 2012a. Interpretation of unsaturated soil behaviour in the stress-saturation space. I: Volume change and water retention behaviour. Computers and Geotechnics, **43**: 178-187. doi: 10.1016/j.compgeo.2012.04.010.

Zhou, A.-N., Sheng, D., Sloan, S.W., and Gens, A. 2012b. Interpretation of unsaturated soil behaviour in the stress-saturation space. II: Constitutive relationships and validations. Computers and Geotechnics, **43**: 111-123. doi: 10.1016/j.compgeo.2012.02.009.

Zhou, A.-N., Sheng, D., and Carter, J.P. 2012c. Modelling the effect of initial density on soil-water characteristic curves. Géotechnique, **62**(8): 669-680. doi: 10.1680/geot.10.P.120.

Zhou, A.-N., and Sheng, D. 2015. An advanced hydro-mechanical constitutive model for unsaturated soils with different initial densities. Computers & Geotechnics, **63**: 46-66. doi: 10.1016/j.compgeo.2014.07.017.

Zhou, A.-N., Huang R.Q., and Sheng, D. 2016. Capillary water retention curve and shear strength of unsaturated soils. Canadian Geotechnical Journal, **53**(6): 974-987. doi: 10.1139/cgj-2015-0322.

Zhou, W.H., Yuen, K.V., and Tan, F. 2014. Estimation of soil-water characteristic curve for granular soils with different initial dry densities. Engineering Geology, **179**(4): 1-9. doi: 10.1016/j.enggeo.2014.06.013.

Table

Table 1 Values of model parameters and initial state variables for Silty sand, Speswhite kaolin and Jossigny silty clay

Material	λ	κ	b_{sw}	M	G_{p0}	Γ_{csat}	a_{Γ}	D	n_p	n_{pt}
Silty sand	0.019	0.003	5.5	1.523	2000	0.56	0.14	1.0	2.5	10.0
Speswhite kaolin	0.11	0.011	3.0	0.793	40	2.000	0.490	0.7	2.0	2.0
Jossigny silty clay	0.08	0.010	1.0	1.16	350	1.142	0.154	0.2	4.0	10.0

Material	λ_w	κ_w	p_a	b_{ws}	S_{rres} (%)	e_0	S_{r0} (%)	$p_c'^{c}$ (kPa)	s_i (kPa)	s_d (kPa)
Silty sand	0.04	0.001	1.0	3.2	45.5	0.347	75.0	450	1000	800
Speswhite kaolin	0.23	0.01	101.3	1.1	25.0	1.206	60.1	210	350	300
Jossigny silty clay	0.21	0.01	101.3	1.5	57.0	0.621	77.0	500	280	180

Figure captions

Figure 1 Yield surfaces in (a) the *p'*-*q* plane and (b) the *p'*-*s* plane

Figure 2 Critical state lines of (a) compacted Speswhite kaolin and (b) Jossigny silty clay

Figure 3 Schematic plot for water retention behaviours

Figure 4 Variations of yield surfaces during (a) drying path and (b) wetting path

Figure 5 Comparison between measured and calculated results for drained triaxial tests at different suctions and net confining stresses on silty sand: (a) deviatoric stress vesus axial strain, (b) specific volume versus axial strain, and (c) degree of saturation versus axial strain

Figure 6 Comparison between measured and calculated results for drained triaxial tests at different suctions and net confining stresses on Speswhite kaolin: (a) deviatoric stress vesus axial strain, (b) specific volume versus axial strain, and (c) degree of saturation versus axial strain

Figure 7 Comparison between measured and calculated results of drained triaxial tests at different net confining stresses and s = 200 kPa on Jossigny silty clay: (a) deviatoric stress vesus axial strain, and (b) volumetric strain versus axial strain

Figure 8 Comparison between measured and calculated results of drained triaxial tests at different net confining stresses and s = 400 kPa on Jossigny silty clay: (a) deviatoric stress vesus axial strain, and (b) volumetric strain versus axial strain

Figure 9 Comparison between measured and calculated results of drained triaxial tests at different net confining stresses and s = 600 kPa on Jossigny silty clay: (a) deviatoric stress vesus axial strain, and (b) volumetric strain versus axial strain

Figure 10 Comparison between measured and calculated results of drained triaxial tests at different net confining stresses and s = 800 kPa on Jossigny silty clay: (a) deviatoric stress vesus axial strain, and (b) volumetric strain versus axial strain

Figure 1

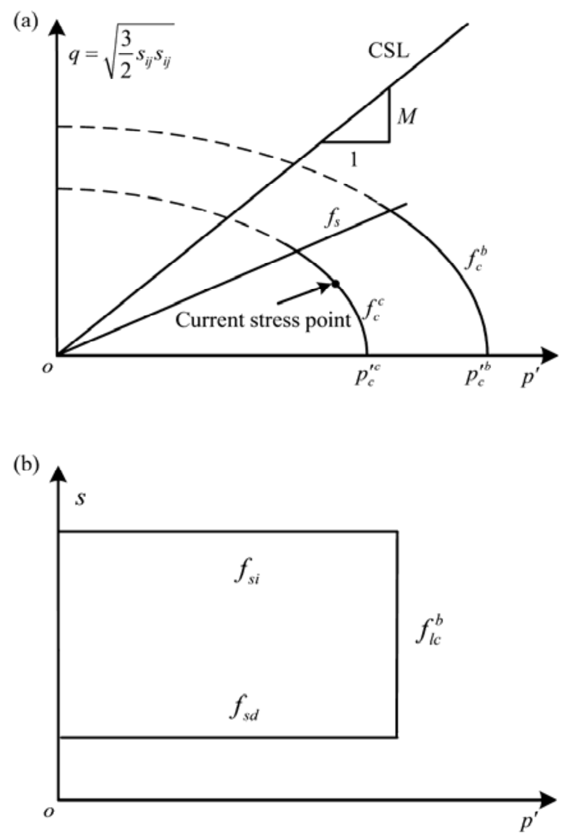

(a)
$q=\sqrt{\frac{3}{2}s_{ij}s_{ij}}$
CSL
M
1
f_s
f_c^b
f_c^c
Current stress point
o
$p_c'^c$
$p_c'^b$
p'
(b)
s
f_{si}
f_{lc}^b
f_{sd}
o
p'

Figure 2

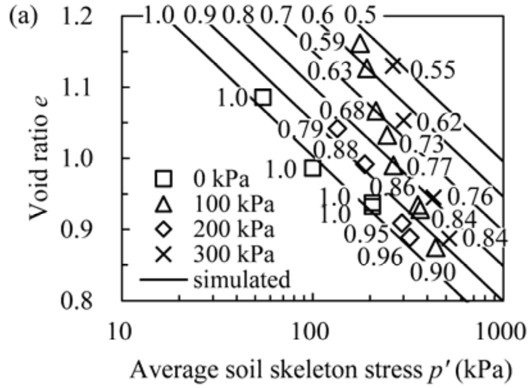

(a)
1.0 0.9 0.8 0.7 0.6 0.5
0.59
0.63
0.55
1.0
0.68
0.62
0.79
0.73
0.88
0.77
1.0
0.86
0.76
1.0
1.0
0.84
0.95
0.84
0.96
0.90
0 kPa
100 kPa
200 kPa
300 kPa
simulated
Void ratio e
Average soil skeleton stress p′ (kPa)

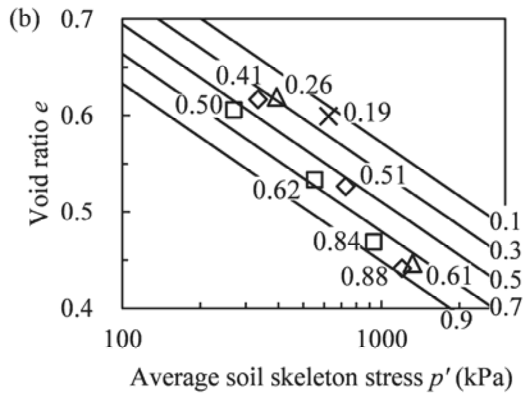

(b)
0.41
0.26
0.50
0.19
0.51
0.62
0.84
0.88
0.61
0.1
0.3
0.5
0.7
0.9
Void ratio e
Average soil skeleton stress p′ (kPa)

Figure 3

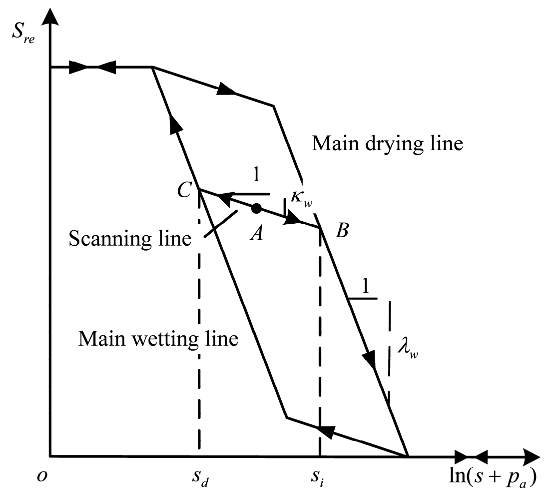

S_{re}
Main drying line
1
κ_w
C
A
B
Scanning line
1
λ_w
Main wetting line
o
s_d
s_i
$\ln(s + p_a)$

Figure 4

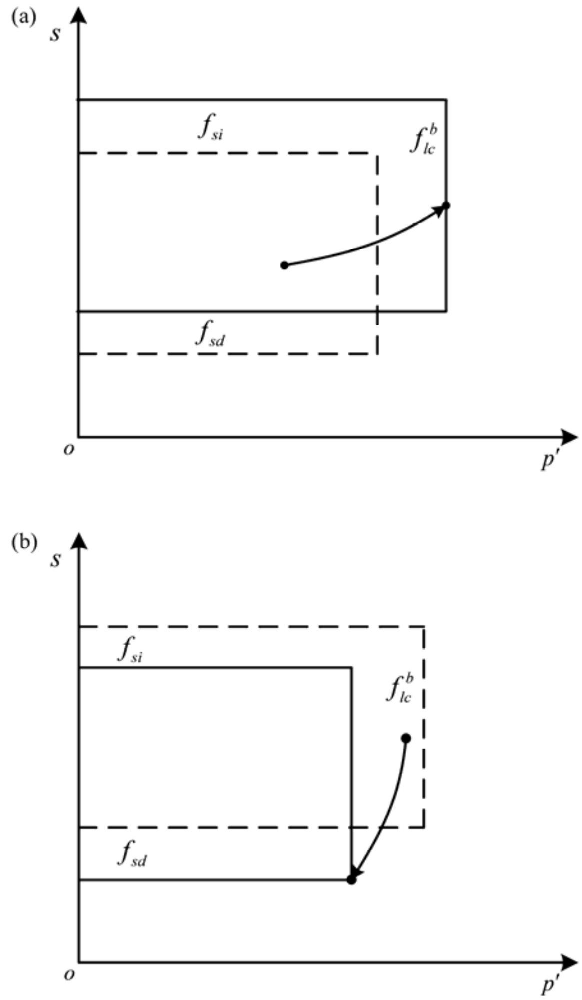

Figure 5

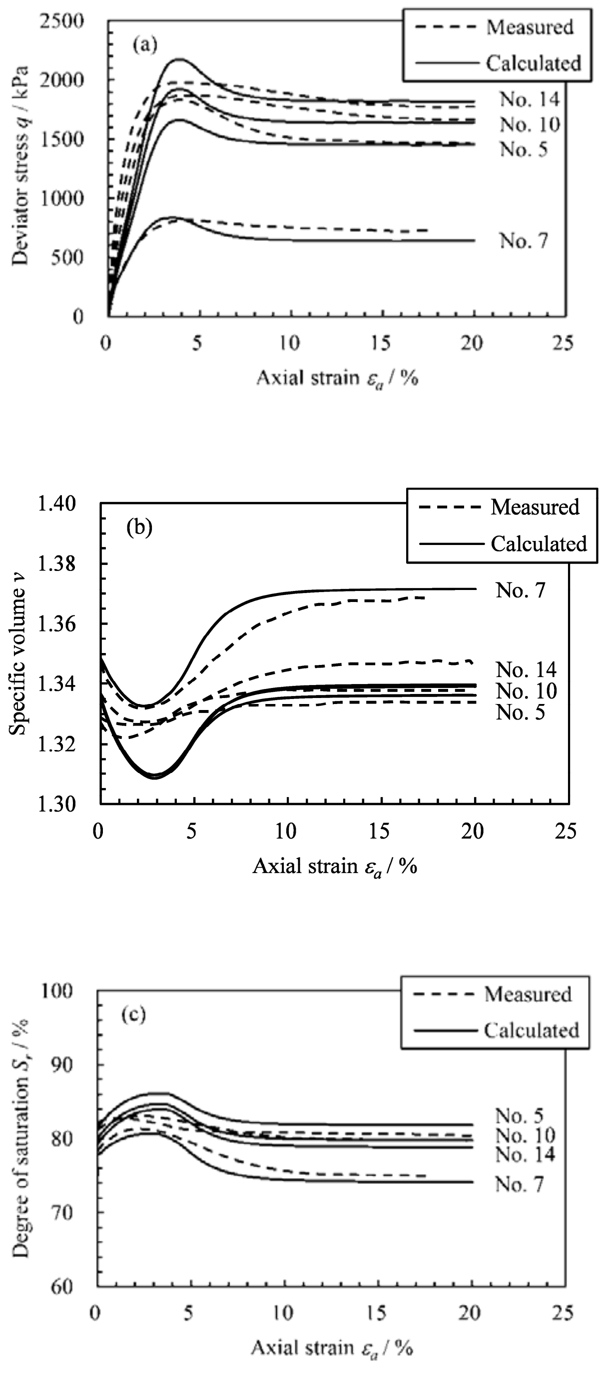

(a)
Measured
Calculated
Deviator stress q / kPa
Axial strain ε_a / %
No. 14
No. 10
No. 5
No. 7
0
500
1000
1500
2000
2500
0
5
10
15
20
25
(b)
Measured
Calculated
Specific volume v
Axial strain ε_a / %
No. 7
No. 14
No. 10
No. 5
1.30
1.32
1.34
1.36
1.38
1.40
0
5
10
15
20
25
(c)
Measured
Calculated
Degree of saturation S_r / %
Axial strain ε_a / %
No. 5
No. 10
No. 14
No. 7
60
70
80
90
100
0
5
10
15
20
25

Figure 6

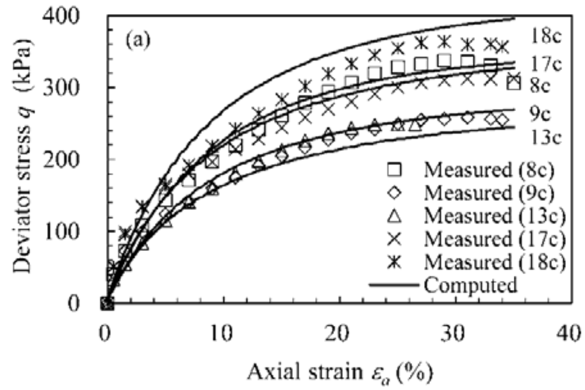

400
300
200
100
0
(a)
Deviator stress q (kPa)
18c
17c
8c
9c
13c
Measured (8c)
Measured (9c)
Measured (13c)
Measured (17c)
Measured (18c)
Computed
0
10
20
30
40
Axial strain ε_a (%)

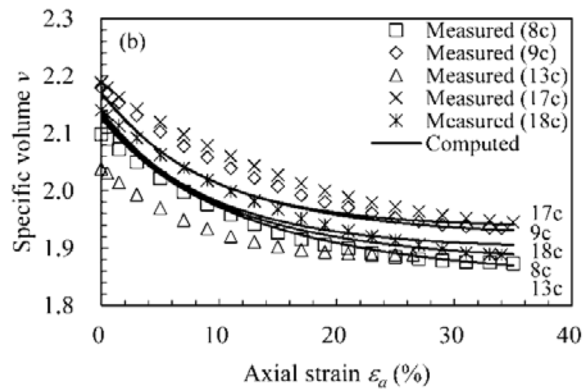

2.3
2.2
2.1
2.0
1.9
1.8
(b)
Specific volume v
Measured (8c)
Measured (9c)
Measured (13c)
Measured (17c)
Measured (18c)
Computed
17c
9c
18c
8c
13c
0
10
20
30
40
Axial strain ε_a (%)

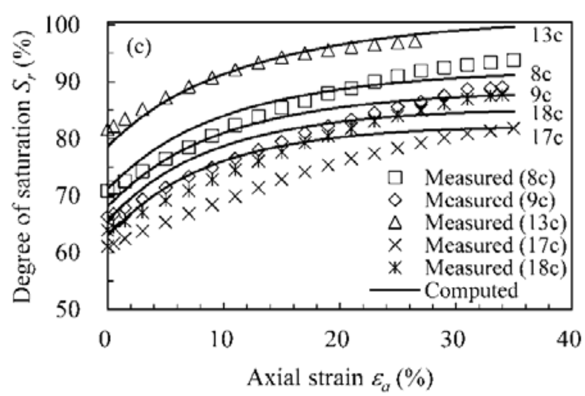

100
90
80
70
60
50
(c)
Degree of saturation S_r (%)
13c
8c
9c
18c
17c
Measured (8c)
Measured (9c)
Measured (13c)
Measured (17c)
Measured (18c)
Computed
0
10
20
30
40
Axial strain ε_a (%)

Figure 7

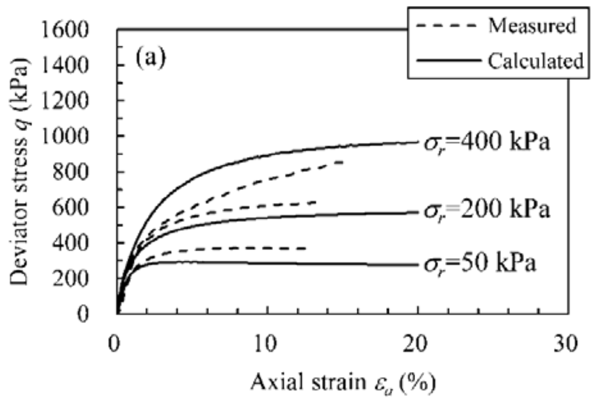

Measured
Calculated
(a)
Deviator stress q (kPa)
Axial strain ε_a (%)
σ_r=400 kPa
σ_r=200 kPa
σ_r=50 kPa
0
200
400
600
800
1000
1200
1400
1600
0
10
20
30

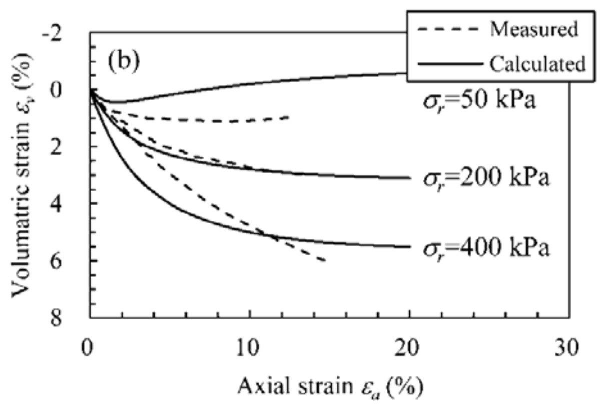

Measured
Calculated
(b)
Volumatric strain ε_v (%)
Axial strain ε_a (%)
σ_r=50 kPa
σ_r=200 kPa
σ_r=400 kPa
-2
0
2
4
6
8
0
10
20
30

Figure 8

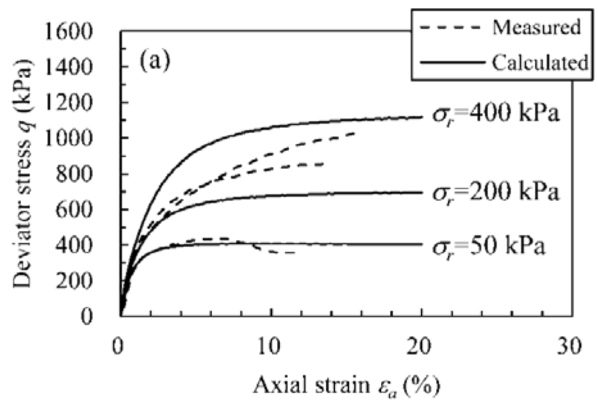

(a)
Measured
Calculated
Deviator stress q (kPa)
Axial strain ε_a (%)
σ_r=400 kPa
σ_r=200 kPa
σ_r=50 kPa

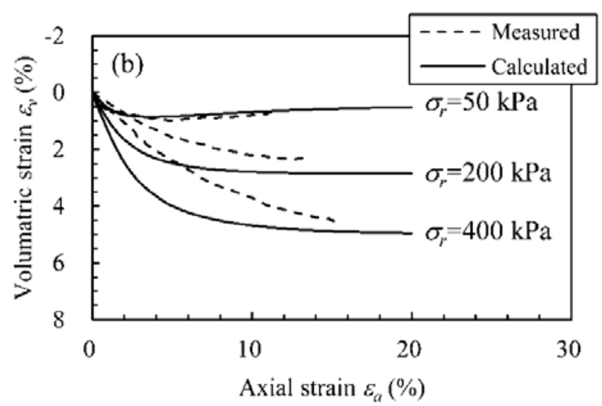

(b)
Measured
Calculated
Volumatric strain ε_v (%)
Axial strain ε_a (%)
σ_r=50 kPa
σ_r=200 kPa
σ_r=400 kPa

Figure 9

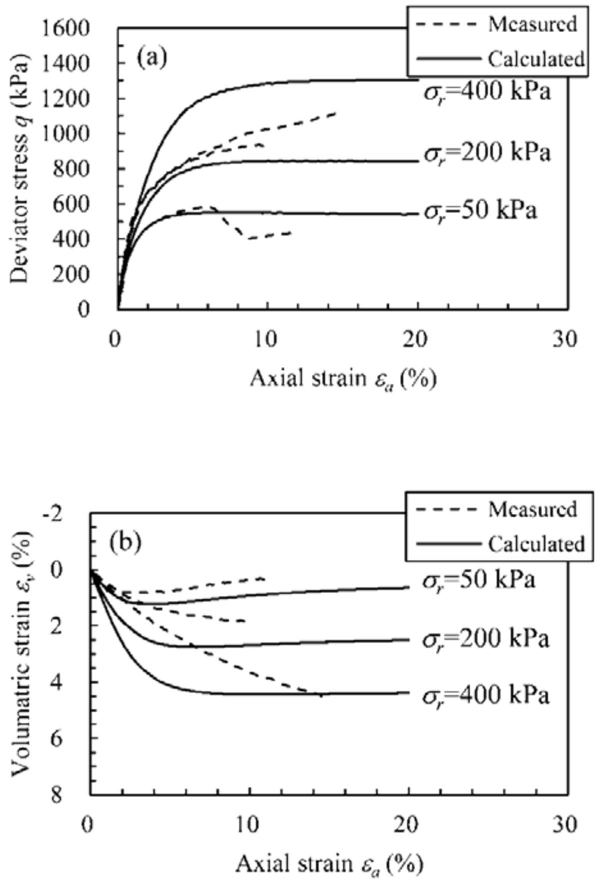

(a)
Measured
Calculated
Deviator stress q (kPa)
1600
1400
1200
1000
800
600
400
200
0
0
10
20
30
Axial strain ε_a (%)
σ_r=400 kPa
σ_r=200 kPa
σ_r=50 kPa
(b)
Measured
Calculated
Volumatric strain ε_v (%)
-2
0
2
4
6
8
0
10
20
30
Axial strain ε_a (%)
σ_r=50 kPa
σ_r=200 kPa
σ_r=400 kPa

Figure 10

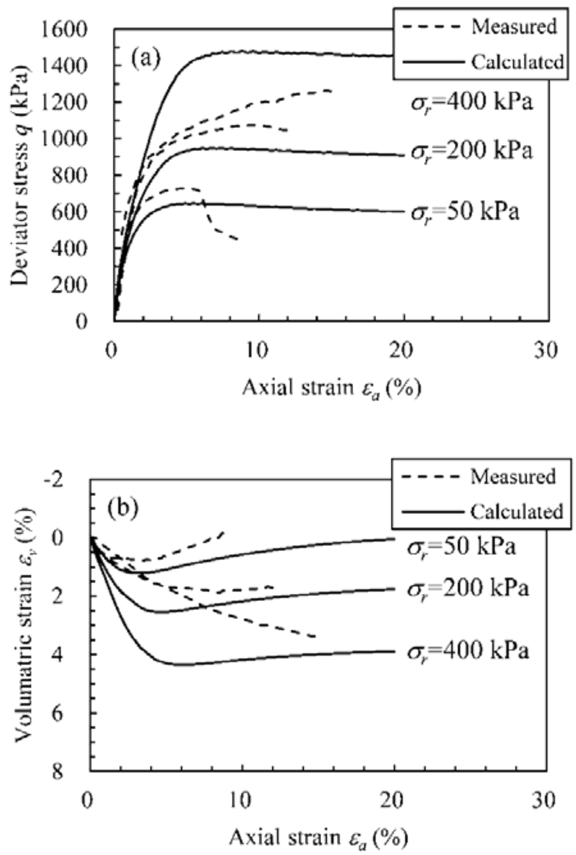
Measured
Calculated
(a)
σ_r=400 kPa
σ_r=200 kPa
σ_r=50 kPa
Deviator stress q (kPa)
Axial strain ε_a (%)
1600
1400
1200
1000
800
600
400
200
0
0
10
20
30
(b)
σ_r=50 kPa
σ_r=200 kPa
σ_r=400 kPa
Volumatric strain ε_v (%)
-2
0
2
4
6
8